RSC Advances

ROYAL SOCIETY OF CHEMISTRY

www.rsc.org/advances

Graphical abstract

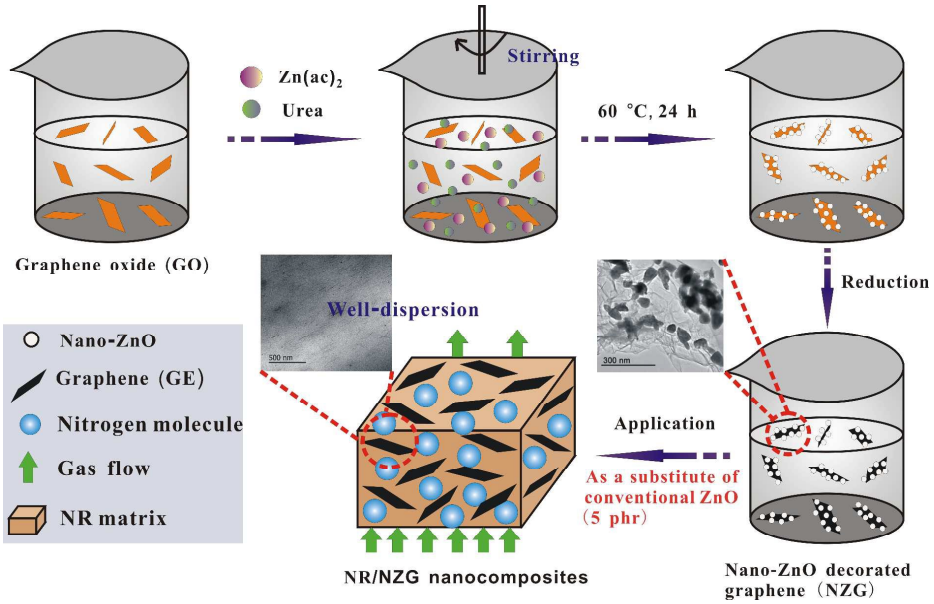

Graphene nanosheets decorated with ZnO nanoparticles: Facile synthesis and promising application for enhancing mechanical and gas barrier properties of rubber nanocomposites

Yong Lin, Zhikai Zeng, Jiarong Zhu, Song Chen, Xue Yuan, Lan Liu*

College of Materials Science and Engineering, Key Lab of Guangdong Province for High Property and Functional Macromolecular Materials, South China University of Technology, Guangzhou 510640, P. R. China.

* *Corresponding author. Tel.: +86 20 87114857; E-mail addresses: psliulan@scut.edu.cn (L. Liu).*

Abstract

In this study, graphene nanosheets decorated with ZnO nanoparticles (NZG) was prepared from graphene oxide by a facile solvothermal method. Simultaneously, NZG as a substitute of conventional ZnO was incorporated into rubber matrix. The NZG not only showed improved vulcanization efficiency but also could simultaneously play the roles of reinforcement for natural rubber (NR) nanocomposites. The results showed that the cure reaction of NR/NZG nanocomposites is significantly faster than that of neat NR. The dynamic and static mechanical properties and the gas barrier property of NR/NZG nanocomposites were systematically investigated at different NZG content. Compared with neat NR, the tensile strength, modulus at 300% strain and tear strength of NR/NZG-2.5 nanocomposite are dramatically enhanced by 67.8%, 188.6% and 74.1%, respectively, at only 2.5 phr NZG content. The permeability of NR/NZG-2.5 nanocomposite decreased by 53% compared to neat NR. The well dispersion of graphene, high vulcanization efficiency of ZnO nanoparticles, together with the enhanced interfacial interaction, is considered to be responsible for the significant synergetic effects in the improvement of the vulcanization characteristic, mechanical performance and the gas barrier property of the composites.

1 Introduction

Over decades rubber nanocomposites have drawn enormous interest and extensive research owing to their attractive properties and promising applications. A notable case concerned is that the practical applications of rubber often require the use of cure activators in the vulcanization to obtain the desired reinforcement, further making rubber composites useful for the wide applications. Nowadays, zinc oxide (ZnO), regarded as an indispensable cure activator, deserves more than passing notice in the vulcanization. It lies in the fact that constituting the network structure is explicitly related to the crosslink, more specifically the cure activation of ZnO.[1,2]

By now, the typical rubber vulcanization recipe contains a maximum of 5 phr (parts per hundred parts of rubber) conventional ZnO, because only thus can it ensure the vulcanization efficiency and enhance the mechanical performance. However, low vulcanization efficiency, consequent of applying it in rubber composites has become a crucial issue. Moreover, ZnO has been divided into a hazardous chemical by some environmental groups and The European Union, toxicity of which seriously threatens the aquatic lives and causes a nonrecoverable damage to the ecological environment. Thereby, the reduction in the quantity of ZnO in rubber composites is sufficient beyond doubt.

To date, ZnO nanoparticles (nano-ZnO), have particularly been a good candidature applied as an effective cure-activator for the vulcanization. Due to its special characteristics such as the “little size effect”, “surface effect” and “quantum effect”,[3,4] the vulcanization efficiency of nano-ZnO can be significantly enhanced by broadening the contacts between the nano-ZnO and the rubber additives in the composites. Therefore, nano-ZnO, a significant contribution to the reduction of ZnO level in rubber composites, has aroused extensive interest for some researchers.[5-7] Nonetheless, the high surface energy

and small size of nano-ZnO have prompted the irreversible aggregation of nanoparticles. Such phenomenon can seriously impede the nano-ZnO usage, and impact the performance of the composites.

In order to obtain the desired performance of rubber composites by incorporation with nano-ZnO, a handy and effective method is required to weaken the aggregation of nano-ZnO. To achieve this objective, the decoration of metal oxide nanoparticles on layered nanomaterials has been exploited as a feasible approach.[8-10] Very recently, graphene (GE) has been examined as an ideal platform for supporting nanoparticles to exploit the metal oxide-GE nanocomposite,[11-14] approach of which mainly focuses on utilizing the GE sheets as carbon mats to anchor metal oxide materials to form new hybrid materials. Such an attachment of metal oxide nanoparticles (ZnO, TiO_2, SnO_2, etc.) onto the GE nanosheets can not only have a tendency to weaken the aggregation clusters of metal oxide, but also eliminate irreversible agglomerates or even restack to form graphite through van der Waals interactions during the synthesis process.[15,16] Also, it has been revealed that when incorporated into polymer matrix[17-19], the GE with the unique structural, physical and chemical properties can remarkably endow those polymer composites with the exceptional performance. Currently, some methods have proven to be useful to produce GE, such as mechanical exfoliation techniques[20], chemical vapor deposition[21], solid-state carbon source deposition[22,23], solution-based reduction of graphene oxide (GO)[24], and nanotube splitting and unzipping[25,26]. For all these processes, considerable interest in the practical application of GE has led to many theoretical and experimental efforts for the large-scale production of GE nanosheets, of particular concern is the most economic solution-based reduction of GO, which has become adopted by most researchers.[27,28] Recently, an effective one-pot method, in which GO sheets and precursor of nano-ZnO are subjected to successive chemical reactions, has been reported to prepare nano-ZnO-graphene (NZG) nanocomposites.[29,30]

Noteworthily, few reports concern the incorporation of NZG into rubber for preparing the rubber/NZG nanocomposites with high performance, thus remain a considerable challenge. It is even possible to predict that NZG, as a promising reinforcement for rubber composites is conducive to exploring the potential application of nanoparticles/GE materials.

In this study, we reported one facile solvothermal method for the synthesis of NZG nanocomposties using GO and $Zn(Ac)_2$ as the precursors for GE and nano-ZnO, respectively. Subsequently, the resultant NZG was incorporated into NR matrix to fabricate NR/NZG nanocomposites. The effects of NZG on the vulcanization characteristic, crosslink network, static and dynamic mechanical properties of NR nanocomposites were addressed. Simultaneously, the relationship between the dispersion state of GE and the overall performance of NR nanocomposites was illustrated and the influence of the GE morphology on the gas permeability of NR nanocomposites was further investigated.

2 Experimental

2.1 Materials

The chemicals used in the experiments are analytical grade reagents without further purification. Natural graphite, Zinc acetate ($Zn(Ac)_2$), ammonia ($NH_3 \cdot H_2O$), hydrazine hydrate, ethanol, acetone and ethylene glycol (EG) were all provided by Guangzhou Chemical Reagent Factory.

All the rubber ingredients were industrial grade and used as received. NR was supplied by Guangzhou Rubber Institute. Zinc oxide, stearic acid, N-cyclohexylbenzothiazole-2-sulphenamide (CZ), 2,2'-dibenzothiazole disulfide (DM), 2-mercaptobenzimidazole (MB) and sulfur were provided by Guangzhou Longsun Technology Co., Ltd.

2.2 Synthesis of NZG nanocomposites

GO was synthesized by a modified Hummers method[31] and ultrasonically-assisted exfoliation. Afterwards, NZG was fabricated by a simple solvothermal method. Typically, 100 mg of GO and 600 mg of $Zn(Ac)_2$ were dispersed in 80 mL of EG under sonication. 1.2 mL of $NH_3{\cdot}H_2O$ and 5 mL DI water were slowly added into the mixture with continuous stirring. The mixture was kept at 60 °C for 24 h. Subsequently, 50 μL of hydrazine hydrate was slowly put into the mixture and maintained at 90 °C for 12 h. The resulted product was isolated by centrifugation, repeatedly washed with water and ethanol, and finally dried in a vacuum oven at 60 °C for 24 h. Then, the as-synthesized NZG powders were obtained after heat-treatment in an atmosphere of air at 600 °C for 6 h. For comparison, GE and nano-ZnO were synthesized in the identical procedure in the absence of $Zn(Ac)_2$ and GO, respectively. In order to measure the weight ratio of GE and nano-ZnO, a desired amount of NZG (m_a) was well dispersed in 1M HCl solution for removing the nano-ZnO. The obtained product (m_b) was isolated by centrifugation, repeatedly washed with water and acetone, and finally dried in a vacuum oven at 60 °C for 24 h. Thereby, the mass fraction φ (wt %) of GE in the NZG powder can be calculated by the equation, $\varphi = (m_b/m_a)*100\%$. Herein, the weight content of GE in the NZG was calculated to be 25 wt%.

2.3 Preparation of NR/NZG nanocomposites

NR was compounded with rubber ingredients in an open two-roll mill and subjected to compression at 143 °C for the optimum curing time determined by a Rubber Process Analyzer. The formulation of NR composite is listed as follow: NR, 100 g; ZnO, 5 g; stearic acid, 2 g; CZ, 1.5 g; DM, 0.5 g; MB, 1.0 g; sulfur, 1.5 g; NZG, variable. The NZG contents in the composites were controlled to be 0.5, 1.0, 1.5, 2.0 and 2.5 phr. As compared, NR composite with 5 phr conventional ZnO (namely, “neat NR”), NR nanocomposites containing up 0.125, 0.250, 0.375, 0.500 and 0.625 phr of GE, and NR nanocomposites

with 0.375, 0.750, 1.125, 1.500 and 1.875 phr of nano-ZnO were also prepared by the same way, respectively. These nanocomposites are abbreviated as "NZG-x", "GE-x" or "Nano-ZnO-x" below. The unknown number x denotes NZG, GE or nano-ZnO content (phr) in the nanocomposites.

2.4 Characterization

X-ray diffraction (XRD) analysis was used to investigate the crystalline structures of NZG, GE and nano-ZnO. The XRD studies were performed with a Bruker D8 Advance X-ray diffractometer with Cu Kα radiation (λ=0.1542 nm). The goniometer scanned diffracted X-rays at a scan speed of $0.15°s^{-1}$. UV-vis absorption spectroscopy was carried out on a UNICAN UV-500 spectrophotometer in ethanol dispersion using a quartz cell with a 1 cm optical path. The evaluation of GE sheets dispersed in NR nanocomposites was made by field emission scanning electron microscope (FESEM, Nova NANOSEM 430) and high resolution transmission electron microscope (HRTEM, JEOL2100). The mechanical properties were all measured by a U-CAN UT-2060 instrument. Tensile tests were performed with dumbbell-shaped specimens according to ASTM D412 with a crosshead speed of 500 mm/min. The tear strength was determined with a right-angle tear die C according to ASTM D624. Crosslink density was recorded by an IIC XLDS-15 HT magnetic resonance crosslink density analyzer. For a swelling test, it was performed by the method reported previously[31]. The bound rubber content in the NR/NZG nanocomposites was determined from the same route as previously[32]. Differential scanning calorimetry (DSC) measurements were performed on a TA Q20 instrument in a nitrogen atmosphere, at a heating rate of 20 °C/min. Dynamic mechanical analysis (DMA) was conducted on a DMA242C dynamic mechanical analyzer in tensile mode. The experiments were conducted in a temperature range of -135 to 75 °C at 3 Hz and heating rate of 3 °C/min. Gas permeability of NR nanocomposites was measured using a gas

permeability tester (VAC-V1, Labthink Instruments). The test gases used were nitrogen, and the samples used were circular-shaped specimens with 50 mm in diameter and 1 mm in thickness.

3 Results and discussion

3.1 Structural characterization of NZG nanocomposites

FESEM was performed to investigate the surface morphology and structure of the samples. As displayed in Fig. 1a, most of GE nanosheets are stacked, curled and entangled together. And the synthesized nano-ZnO exhibits an obvious tendency for the nanoparticles to agglomerate, as shown in Fig. 1b. Noteworthily, Fig. 1(c-d) draws the FESEM images of NZG nanocomposites. It should be noted that the surface of the curled GE nanosheets is covered by densely packed and irregularly shaped nano-ZnO in a large-scale, which implies a good combination between GE nanosheets and nano-ZnO. Interestingly, some nano-ZnO particles are grown on the brink of interlayer and inside interlayer of GE nanosheets, resulting in the wrinkled textures to form a sandwich-like GE-ZnO structure to avoid the restack of GE nanosheets. Simultaneously, the EDS spectrum (the inset of Fig. 1d) does prove that Zn atom exists in the nanocomposites and no impurities have been introduced into the nanocomposites.

Fig. 1(e-f) illustrates the TEM images of NZG nanocomposites. The GE nanosheets are decorated by nano-ZnO with 100 nm in diameter. Notably, some nano-ZnO particles are dispersed on the surface of the wrinkled GE nanosheets and some are covered or wrapped by thin GE nanosheets, in agreement with the FESEM observations.

The phase and structure of the synthesized samples were further detected by XRD. As shown in Fig. 2a, the XRD pattern of the synthesized NZG nanocomposites shows the diffraction peaks at 31.6°, 34.4°, 36.1°, 47.3°, 56.3°, 62.6°and 67.6°, ascribed to (100), (002), (101), (102), (110), (103) and (112) planes

of ZnO, phenomenon of which is consistent with those of nano-ZnO. These results show that both of the synthesized nano-ZnO and the nano-ZnO decorated onto the GE nanosheets can be mainly ascribed to a hexagonal phase ZnO and appear the excellent crystal structures. And no any obvious characteristic peaks corresponding to GO and graphite were observed. In contrast, it is found that the GE shows a new and broad (002) diffraction peak at 2θ=24.02°, suggesting that the GE nanosheets were inclined to the aggregation after reduction. This result indicates that the decoration of nano-ZnO on the surfaces of GE nanosheets can effectively inhibit the agglomeration of GE.

Fig. 2b displays the UV-vis absorption spectra of the synthesized NZG nanocomposites, together with GE and nano-ZnO for comparison. It can be clearly seen that the GE shows a strong absorption peak at 265 nm, generally regarded as the excitation of π-plasmon of graphitic structure.[33] And a strong absorption peak located at 376 nm is observed for the nano-ZnO.[33,34] Noteworthily, compared with GE and nano-ZnO, the absorption peaks assigned to GE and ZnO were shifted to 277 nm and 367 nm in the NZG nanocomposites, respectively. The shifts in the absorption peaks can be attributed to a coupling effect,[29,35] demonstrating a strong interaction between GE and nano-ZnO. Such result can also be confirmed by XPS analysis (see Fig. S1 of supporting information). The negative shifts in the binding energies for Zn2p3/2 and Zn2p1/2 are clearly occurred because of the interaction between nano-ZnO and GE. Additionally, the difference of C1s spectra between GO and NZG suggests the most of oxygen-containing functional groups have been removed after reduction.

3.2 Morphology of NR/NZG nanocomposites

The dispersion status of GE in the NR nanocomposites was evaluated by FESEM and HRTEM. The FESEM images of cryogenically fractured surfaces for neat NR and NR/NZG-2.5 nanocomposite are

compared in Fig. 3a,b. The surface of neat NR is smooth in the view. With the incorporation of NZG into the matrix, the sample exhibits the rough fractured surfaces with protuberances. These protuberances are derived from the introduced GE nanosheets wrapped by NR chains. HRTEM was used to directly visualize the dispersed GE nanosheets in the matrix. As for NR/GE-0.625 nanocomposite, the apparent stacking of GE nanosheets is observed in Fig. 3c. This may be due to that the aggregation of GE nanosheets can be occurred before latex coagulation. However, the comparison on the dispersion status of GE in the NR/NZG-2.5 nanocomposite (contents 0.625 phr GE) is displayed in Fig. 3d. It is noticed that the GE nanosheets are finely dispersed throughout the matrix, and exist as individual layers without the aggregates. These results provide the clear evidence that the nano-ZnO covered on GE nanosheets effectively hinder the aggregation of GE during the mill-mixing process and vulcanization process. Additionally, the XRD analysis (see Fig. S2 of supporting information) also reveals that nano-ZnO decorated on the GE facilitates the GE dispersed in the matrix, and NZG with a low content has a higher vulcanization efficiency compared with 5 phr conventional ZnO.

3.3 Vulcanization characteristics and network structure of NR/NZG nanocomposites

The effect of NZG on the vulcanization characteristics of NR nanocomposites has been analyzed, as well as a composite containing 5 phr conventional ZnO. The vulcanization characteristics of NR nanocomposites are expressed in term of the scorch time (T_{10}), optimum curing time (T_{90}), minimum torque (M_L), and maximum torque (M_H). As depicted in Fig. 4, it can be seen that all vulcanization characteristics increase with increasing NZG content. The results indicate that the presence of NZG in the NR nanocomposites extend the incipient vulcanization and curing time of the vulcanization. The torque of NR nanocomposites is increasing with increasing NZG content, which is proportional to the formation of

crosslink network and the strong interfacial interactions between GE nanosheets and the matrix.[36,37] However, it is noteworthy mentioning that NZG with low content (0.5 or 1 phr) causes a reduction of vulcanization characteristics in comparison with 5 phr conventional ZnO, demonstrating that such NZG content can not effectively facilitate the vulcanization. This phenomenon may be contributed to that the low content of NZG can not sufficiently promote the formation of the zinc salts of stearic acids, which play a important role in solubilizing those insoluble accelerators to form the actual catalyst for vulcanization process. With that, higher content of NZG results in a significant increase in M_L and M_H. Meanwhile, the cure rate index (CRI) and the difference between M_H and M_L (ΔS) are presented in Fig. 4c. CRI of NR/NZG nanocomposites are significantly higher than that of NR composite containing 5 phr conventional ZnO, suggesting that NR can be crosslinked rapidly with the inclusion of NZG. These results are due to that nano-ZnO has a larger surface area than conventional ZnO, and therefore it has a tendency to accelerate the reactions between nano-ZnO, stearic acid and accelerators. Such result prominently favors the vulcanization, allowing sulfur insertion to occur more rapidly.[38] And ΔS values have an increase with increasing NZG content, which is closely associated with the crosslink degree of network structure of NR composites. The contribution of NZG on the crosslink network is also validated by swelling measurements in Fig. S3 of supporting information. Thereby, these results convincingly show that NZG can behave as an effective cure activator in the vulcanization.

To further investigate the effect of NZG on the network structure of NR nanocomposites, DSC was adopted to analyze the glass transition of NR/NZG nanocomposites as illustrated in Fig. 5a, and the results are listed in Table 1. An increase of T_g is obviously observed. Such trend indicates that the well dispersion of GE and excellent vulcanization efficiency of nano-ZnO can lead to the enhanced network

structure. Also, it is clearly seen that ΔC_p decreases systematically with increasing NZG content, which reflects a decrease of the chains mobility due to its interaction with the GE nanosheets. Similar results in polyurethane/clay composites[39] and poly(dimethylsiloxane)/silica composites[40] have been interpreted in terms of a fraction of polymer being immobilized on the surface of fillers. In order to follow that point, the weight fraction of immobilized NR (χ_{im}) was calculated by the following equation[41]:

$$\Delta C_{pn} = \Delta C_p / (1-\omega) \quad (1)$$

$$\chi_{im} = (\Delta C_{p0} - \Delta C_{pn}) / \Delta C_{p0} \quad (2)$$

Where ΔC_{p0} refers to the heat capacity jump at T_g of neat NR, ΔC_p is on behalf of the heat capacity jump at T_g of NR/NZG nanocomposites, ΔC_{pn} represents the heat capacity jump at T_g of NR nanocomposites normalized to the rubber fraction, and ω is the weight fraction of GE in the nanocomposites.

By calculation, DSC results are listed in Table 1 and χ_{im} is plotted as a function of ω in Fig. 5b. χ_{im} tends to increase with increasing ω, and such increase is moderate in view of the large variation of ω. The changed immobilized NR (χ_{im}) reflects the NR chains mobility affected by the interfacial interaction between the chains and the GE nanosheets. The higher the value of χ_{im}, the stronger the interfacial interaction between NR and GE. The underlying mechanism regarding the enhancement in the interfacial interactions is attributed to that GE even after reduction bears -OH and -COOH groups, which can be converted into thiol (-SH), thioester (-CSOR), and dithiocarboxylic ester (-CSSR) groups upon reaction with sulfur. These formed groups interact with accelerator and sulfur, thus the polysulfides species are generated to attack the unsaturated sites on the rubber chains and form a complex crosslink network.[42,43] Moreover, nano-ZnO decorated onto the GE nanosheets has a larger surface area than conventional ZnO, which prominently favors the vulcanization and then efficiently enhances the interfacial adhesion

between the GE nanosheets and NR matrix. Thus, the rubber chains in the interfacial layer are effectively anchored or attached to the surface of GE nanosheets, result of which leads to the strong interfacial interactions between the GE nanosheets and NR matrix.

In order to deeply verify the interfacial interaction, the results of bound rubber are illustrated in Fig. 5c, wherein the degree of rubber-GE interaction was measured by bound rubber content. It is apparent that bound rubber content significantly increases for the rubber compounds with raising the NZG content, indicating that the rubber-GE interaction is enhanced by the increased NZG content. This variation is attributed to that the well-dispersion of GE in rubber matrix can amplify the contact areas between NR and GE, thereupon makes the rubber chains more efficiently attached to the GE.

3.4 Mechanical properties of NR/NZG nanocomposites

Following the excellent activator efficiency of NZG towards NR composites, the effect of NZG, GE and nano-ZnO on the mechanical properties of NR nanocomposites were experimentally investigated, emphasizing the superiority of NZG in the enhancement of nanocomposites. As depicted in Fig. 6, the results reveal that, as compared with NR/Nano-ZnO-1.875 nanocomposite, the tensile strength, modulus at 300% strain and tear strength of NR/NZG-2.5 nanocomposite substantially increase by 18.3% (from 28.12 to 33.26 MPa), 68.6% (from 2.55 to 4.30 MPa) and 14.6% (from 30.27 to 34.68 kN/m), respectively. As a fascinating carbonaceous material, GE exhibits versatile characteristics for improving the performance of NR nanocomposites. An enhancement of the maximum strength is obtained as GE content is gradually increasing. It is of interest to note that the NR/NZG-2.5 nanocomposite (contents 0.625 phr GE) provided a higher mechanical properties than that of NR/GE-0.625 nanocomposite using 5 phr conventional ZnO as the cure activator. For example, the tensile strength of the NR/NZG-2.5

nanocomposite is up to 33.26 MPa, a 6.5% enhancement compared with that of NR/GE-0.625 nanocomoposite. For all the cases, the modulus increment is significant accompanied with a relatively noticeable decrease in elongation at break. Noteworthily, compared with neat NR filled with 5 phr conventional ZnO, the tensile strength, modulus at 300% strain and tear strength of NR/NZG-2.5 nanocomposite are dramatically enhanced to 33.26 MPa, 4.30 MPa and 34.68 kN/m, increasing by 67.8%, 188.6% and 74.1%, respectively. For explaining this phenomenon, the mechanical properties of composites are closely associated with the specific surface areas of the samples. As shown in Table S1 of supporting information, the specific surface areas of conventional ZnO is only 6.046 m^2/g, while the specific surface areas of NZG is up to 35.566 m^2/g. The large surface area is conducive to promote the formation of the soluble sulfurating complex for the vulcanization. So an increase in vulcanization efficiency affected by the specific surface area of the fillers results in increasing vulcanization reactions and improvements of the mechanical properties of the composites. Noteworthily, the specific surface areas of NZG (35.566 m^2/g) is larger than that of Nano-ZnO (31.253 m^2/g), directly indicating that ZnO nanoparticles decorated onto the GE sheets can efficiently reduce the aggregation tendency. Therefore, NR/NZG nanocomposites filled with lower NZG content can exhibit superior mechanical properties to those of neat NR and NR/Nano-ZnO nanocomposites. Additionally, for further reflecting the reinforcement of NZG towards NR, the mechanical properties of NR composites prepared by physically adding rGO and ZnO (NR/rGO/ZnO composites) were provided in Fig. S4 of supporting information. It is clearly seen that NR/NZG nanocomposites show the improved mechanical properties to those of NR/rGO/ZnO composites at the same filler content. Accordingly, NZG has much stronger reinforcement effect on the mechanical performance of NR nanocomposites compared with GE and nano-ZnO, and such

enhanced mechanical properties make NZG very competitive for potential applications as the effective cure activator in the vulcanization.

The underlying mechanism regarding the increases in the mechanical properties of NR nanocomposites and displaying the superiority of NZG in the enhancement of overall performance is attributed to that (a) the well dispersion of GE nanosheets in the matrix can preclude the stress concentration of the cracks and dissipate energy during the loading situation, (b) the strong interfacial interaction between GE and NR can promote a very efficient load transfer from the matrix to GE nanosheets, and (c) the nano-ZnO decorated on the GE nanosheets, possesses the large surface area, which can achieve the maximization of vulcanization efficiency by broadening the contacts between the nano-ZnO and rubber additives, and promote the formation of crosslink network. Therefore, the impressive enhancement in the mechanical properties of NR/NZG nanocomposites should be ascribed to the incorporation of well-dispersed GE, the fine interfacial structure and the high vulcanization efficiency of nano-ZnO.

3.5 Reinforcing efficiency of NZG on NR nanocomposites

To further study on the reinforcing efficiency of NZG as well as the structure information of the nanocomposites, DMA measurement was carried on neat NR and NR/NZG nanocomposites. Fig. 7 shows the variation of storage modulus (E') and the loss factor (tan δ) at 3 Hz as a function of temperature (-135 °C ~ 75 °C) for NR nanocomposites. The E' of NR nanocomposites are generally improved with increasing NZG content (>1.0 phr) at low temperature ranges, which shows that NZG can effectively reinforce the NR. With increasing the temperature, the E' suddenly drop down by 3 orders of magnitude corresponding to the glass-rubber transition of NR chains. This drop can be assigned to an energy

dissipation phenomenon.[19,44] It is apparent that the maximum value of tan δ has a decrease with increasing NZG content and the location of the peak shifts to higher temperature, which reflects the restricted rubber chains due to strong interfacial interaction between GE and rubber.[36,44] Additionally, the decrease in the maximum value of tan δ was positively correlated with the enhanced interfacial interaction.[45] For further evaluating the interfacial interaction between GE and NR matrix, the relationship between the tan δ values of neat NR and NR/NZG nanocomposites can be calculated by using the following equation[46].

$$\tan\delta = \frac{\tan\delta_m}{1+1.5B\Phi}$$

where tan δ and tan δ_m represent the maximum value of tan δ for neat NR and NR/NZG composites, respectively. B is an interaction parameter, the larger the value, the stronger the interfacial interaction between NR matrix and GE. Φ is the volume fraction of GE.

According to the temperature dependence of tan δ of NR nanocomposites with different NZG content shown in Fig. 7b, the maximum value of tan δ of NR/NZG nanocomposites is decreased with increasing NZG content. And the evolution of B with NZG content is plotted in Fig. 7c. Noticeably, the B value is increased with increasing NZG content, suggesting consistently enhanced interfacial interaction.

Observations have shown that the GE nanosheets can be well dispersed through the NR matrix and a strong interfacial interaction between GE and NR matrix has been evidenced. We expected that NR/NZG nanocomposites should have potential application in gas-resistant materials. Nitrogen permeability of NR/NZG and NR/GE nancomposites as a function of GE content is shown in Fig. 8a. It clearly exhibits a significant decrease in the permeability for NR/GE nanocomposites with increasing NZG content. The permeability is decreased by 45% for NR/GE-0.625 nanocomposite by comparing with that of neat NR. It is also worth mentioning that a more significant decrease in the permeability of the NR/NZG

nanocomposites is observed with the inclusion of NZG. For example, the permeability of NR/NZG-2.5 at a GE content of 0.625 phr dramatically decreased by 53% compared to that of neat NR.

It is believed that the reductions in the gas permeability of NR nanocomposites can be largely associated with the dispersion of GE nanosheets and the interfacial interaction. Therefore, on the basis of the observed morphologies of the GE nanosheets (Fig. 3), a model was proposed to present the efficient network for gas flow in NR nanocomposites shown in Fig. 8(b-d). It clearly explained that the NZG exhibited higher enhancement in gas barrier property by comparing with GE. As seen from Fig. 8a, neat NR has high gas flux across the matrix without the inclusion of layered materials. With the incorporation of NZG and GE into the matrix, the tortuous diffusion path is formed owing to high aspect ratio of GE as shown in the schematic diagram of Fig. 8(b-c). Nevertheless, the HRTEM results show that the GE in NR/NZG nanocomposites exhibits better dispersion state in comparison with that in NR/GE nanocomposites. The well-dispersion of GE is the significant factor contributing to a reduced cross section and a tortuous diffusion path,[47,48] greatly interfering with the gas transport throughout the matrix. Importantly, the strong interfacial interaction also plays a key role in lessening the free volume at the interface, which is conducive to reduction in the gas permeability.[49] Additionally, the gas permeability of graphene, graphene oxide, graphite derivative/elastomer nanocomposites is listed in Table 2. As compared with those values reported in the literature for elastomer-graphene nanocomposites, NZG is potentially employed as a good candidate for gas-resistant materials with high performance.

4 Conclusions

Graphene nanosheets decorated with ZnO nanoparticles (NZG) were successfully synthesized by one facile solvothermal method in this study. Characterizations demonstrated that ZnO nanoparticles

(nano-ZnO) are successfully anchored onto graphene (GE) sheets. Simultaneously, NZG as a substitute of conventional ZnO were incorporated into NR matrix and the influence of NZG on the vulcanization characteristic, dynamic and static mechanical properties and the gas permeability of the obtained NR/NZG nanocomposites were investigated. The results showed that low NZG content possesses a higher vulcanization efficiency and much stronger reinforcement effect on the mechanical performance and gas barrier properties of NR nanocomposites compared with GE, nano-ZnO and 5 phr conventional ZnO, results of which are positively correlated with the well dispersion of GE throughout the NR matrix, the enhanced interfacial interaction between the GE and the matrix, and the high vulcanization efficiency of nano-ZnO. Accordingly, NZG with lower content exhibits very competitive for preparing the rubber composites with high performance, and may be regarded as a substitute of 5 phr conventional ZnO for application in rubber composites.

Acknowledgments

The authors gratefully acknowledge "National Basic Research Program of China (No. 2015CB654700 (2015CB654703))", "National Natural Science Foundation of China" (U1134005), "Strategic New Industry Core Technology Research Project of Guangdong Province" (2012A090100017) and "National Undergraduate Training Programs for Innovation" (201410561037) for the financial support.

References

1 B. Panampilly and S. Thomas, *Polym. Eng. Sci.*, 2013, **53**, 1337-1346.

2 Z. H. Li, J. Zhang and S. J. Chen, *Express Polym. Lett.*, 2008, **2**, 695-704.

3 Z. L. Peng, Y. Zhang and X. Liang, *Polym. Polym. Compos.*, 2001, **9**, 275-282.

4 J. Z. Zhang, X. Wang, L. D. Lu, D. Li and X. J. Yang, *J. Appl. Polym. Sci.*, 2003, **87**, 381-385.

5 N. Vatansever and S. Polat, *Mater. Design.*, 2010, **31**, 1533-1539.

6 L. Li, J. Zhang, J. O. Jo, S. Datta and J. K. Kim, *Mater. Design.*, 2013, **49**, 922-928.

7 I. J. Kim, W. S. Kim, D. H. Lee, W. Kim and J. W. Bae, *J. Appl. Polym. Sci.*, 2010, **117**, 1535-1543.

8 A. K. Roy, B. Park, K. S. Lee, S. Y. Park and I. In, *Nanotechnology*, 2014, **25**, 445603.

9 A. K. Roy, S. Y. Park and I. In, *Nanotechnology*, 2015, **26**, 105601.

10 Y. J. Kim, J. H. Lee and G. C. Yi, *Appl. Phys. Lett.*, 2009, **95**, 213101.

11 B. Jaleh and A. Jabbari, *Appl. Surf. Sci.*, 2014, **320**, 339-347.

12 T. N. Lambert, C. A. Chavez, B. Hernandez-Sanchez, P. Lu, N. S. Bell, A. Ambrosini, T. Friedman, T. J. Boyle, D. R. Wheeler and D. L. Huber, *J. Phys. Chem. C.*, 2009, **113**, 19812-19823.

13 C. Nethravathi, T. Nisha, N. Ravishankar, C. Shivakumara and M. Rajamathi, *Carbon*, 2009, **47**, 2054-2059.

14 F. H. Li, J. F. Song, H. F. Yang, H. S. Gan, Q. X. Zhang and D. Han, *Nanotechnology*, 2009, **20**, 455602.

15 G. Williams, B. Seger and P. V. Kamat, *ACS Nano.*, 2008, **2**, 1487-1491.

16 S. M. Paek, E. J. Yoo and I. Honma, *Nano Lett.*, 2009, **9**, 72-75.

17 L. Gan, S. M. Shang, C. W. M. Yuen and S. X. Jiang, *RSC Adv.*, 2015, **5**, 15954-15961

18 G. Scherillo, M. Lavorgna, G. G. Buonocore, Y. H. Zhan, H. S. Xia, G. Mensitieri and L. Ambrosio, *ACS Appl. Mater. Inter.*, 2014, **6**, 2230-2234.

19 H. S. Yang, P. Liu, T. P. Zhang, Y. X. Duan and J. M. Zhang, *RSC Adv.*, 2014, **4**, 27687-27690.

20 K. S. Novoselov, A. K. Geim, S. V. Morozov, D. Jiang, Y. Zhang, S. V. Dubonos, I. V. Grigorieva and A. A. Firsov, *Science* 2004, **306**, 666-669.

21 A. Reina, X. Jia, J. Ho, D. Nezich, H. B. Son, V. Bulovic, M. S. Dresselhaus and J. Kong, *Nano Lett.*, 2008, **9**, 30-35.

22 G. Ruan, Z. Sun, Z. Z Peng and J. M. Tour, *ACS Nano*, 2011, **5**, 7601-7607.

23 Z. Yan, Z. W. Peng, Z. Z. Sun, J. Yao, Y. Zhu, Z. Liu, P. M. Ajayan and J. M. Tour, *ACS Nano* 2011, **5**, 8187-8192.

24 N. Behabtu, J. R. Lomeda, M. J. Green, A. L. Higginbotham, A. Sinitskii, D. V. Kosynkin, D. Tsentalovich, A. N. G. Parra-Vasquez, J. Schmidt, E. Kesselman, Y. Cohen, Y. Talmon, J. M. Tour and M. Pasquali, *Nat. Nanotechnol.*, 2010, **5**, 406-411.

25 D. V. Kosynkin, A. L. Higginbotham, A. Sinitskii, J. R. Lomeda, A. Dimiev, B. K. Price and J. M. Tour, *Nature*, 2009, **458**, 872-876.

26 D. V. Kosynkin, W. Lu, A. Sinitskii, G. Pera, Z. Z. Sun and J. M. Tour, *ACS Nano*, 2011, **5**, 968-974.

27 D. Ponnamma, K. K. Sadasivuni, M. Strankowski, P. Moldenaers, S. Thomas and Y. Grohens, *RSC Adv.*, 2013, **3**, 16068-16079.

28 S. Park and R. S. Ruoff, *Nat. Nanotechnol.*, 2009, **4**, 217-224.

29 J. L. Wu, X. P. Shen, L. Jiang, K. Wang and K. M. Chen, *Appl. Surf. Sci.*, 2010, **256**, 2826-2830.

30 T. Lu, L. K. Pan, H. B. Li, G. Zhu, T. Lv and X. J. Liu, *J. Alloy. Comp.*, 2011, **509**, 5488-5492.

31 H. L. Kang, K. H. Zuo, Z. Wang, L. Q. Zhang, L. Liu and B. C. Guo, *Compos. Sci. Technol.*, 2014, **92**, 1-8.

32 S. Wolff, M. J. Wang and E. H. Tan, *Rubber Chem. Technol.*, 1993, **66**, 163-177.

33 X. Wang, L. J. Zhi, N. Tsao, Z. Tomovic, J. L. Li and K. Mullen, *Angew. Chem. Int. Edit.*, 2008, **47**, 2990-2992.

34 L. Xing and X. Zhang, *J. Phys. Chem. C*, 2007, **111**, 9081-9085.

35 R. C. Wang, Y. C. Chen, S. J. Chen and Y. M. Chang, *Carbon*, 2014, **70**, 215-223.

36 T. Muraleedharan, M. G. Kumaran and G. Unnikrishnan, *J. Appl. Polym. Sci.*, 2004, **93**, 2606-2621.

37 Z. H. Tang, X. H. Wu, B. C. Guo, L. Q. Zhang and D. M. Jia, *J. Mater. Chem.*, 2012, **22**, 7492-7501.

38 A. Y. Coran, *J. Appl. Polym. Sci.*, 2003, **87**, 24-30.

39 S. Kripotou, P. Pissis, Y. V. Savelyev, L. P. Robota and T. V. Travinskaya, *J. Macromol. Sci. B*, 2010, **49**, 86-110.

40 D. Fragiadakis, P. Pissis and L. Bokobza, *Polymer*, 2005, **46**, 6001-6008.

41 R. Ruggerone, V. Geiser, S. D. Vacche, Y. Leterrier and J. A. E. Manson, *Macromolecules*, 2010, **43**, 10490-10497.

42 N. Yan, G. Buonocore, M. Lavorgna, S. Kaciulis, S. K. Balijepalli,Y. H. Zhan, H. S. Xia and L. Ambrosio, *Compos. Sci. Technol.*, 2014, **102**, 74-81.

43 Wu, J.R., Xing, W., Huang, G.S., Li, H., Tang, M.Z., Wu, S.D. and Liu, Y.F., *Polymer*, 2013, **54**, 3314-3323.

44 S. Bhattacharyya, C. Sinturel, O. Bahloul, M. L. Saboungi, S. Thomas and J. P. Salvetat, *Carbon*, 2008, **46**, 1037-1045.

45 E. Vassileva and K. Friedrich, *J. Appl. Polym. Sci.*, 2003, **89**, 3774-3785.

46 K. D. Ziegel and A. Romanov, *J. Appl. Polym. Sci.*, 1973, **17**, 1119-1131.

47 J. R. Wu, G. S. Huang, H. Li, S. D. Wu, Y. F. Liu and J. Zheng, *Polymer*, 2013, **54**, 1930-1937.

48 E. P. Giannelis, *Adv. Mater.*, 1996, **8**, 29-35.

49 Y. Q. Wang, Y. P. Wu, H. F. Zhang, L. Q. Zhang, B. Wang and Z. F. Wang, *Macromol. Rapid Comm.*,

2004, **25**, 1973-1978.

50 W. Xing, M. Z. Tang, J. R. Wu, G. S. Huang, H. Li, Z. Y. Lei, X. Fu and H. Y. Li, *Compos. Sci. Technol.*, 2014, **99**, 67-74.

51 J. Yang, M. Tian, Q. Jia, J. Shi, L. Zhang, S. Lim, Z. Yu and Y. Mai, *Acta Mater.*, 2007, **55**, 6372-6382.

52 H. Kim, Y. Miura and C. W. Macosko, *Chem. Mater.*, 2010, **22**, 3441-3450.

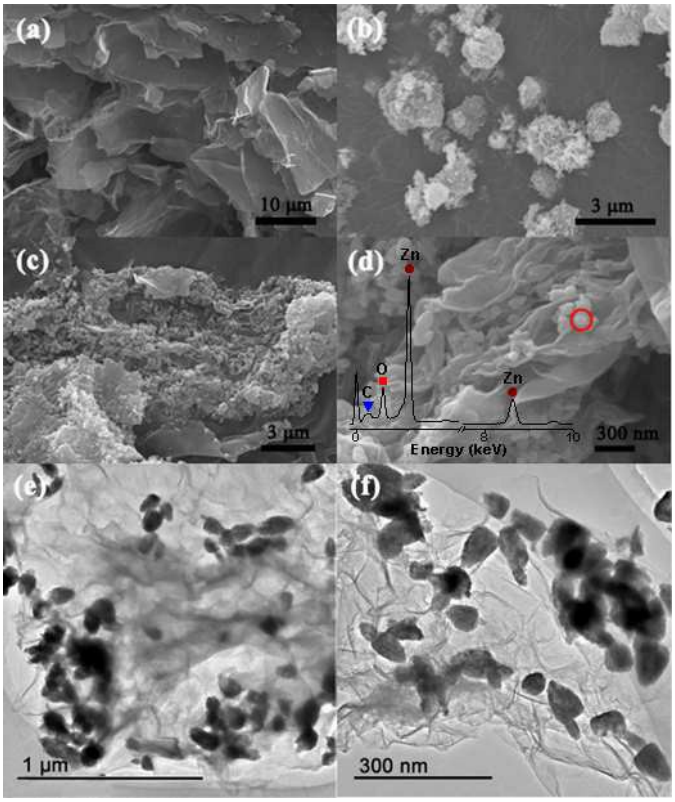

Fig. 1 (a-d) FESEM images of GE (a), nano-ZnO (b) and NZG nanocomposites (c-d). The inset in (d) is the EDS spectra corresponding to the circle-marked region of NZG nanocomposites in (d). (e-f) TEM images of NZG nanocomposites.

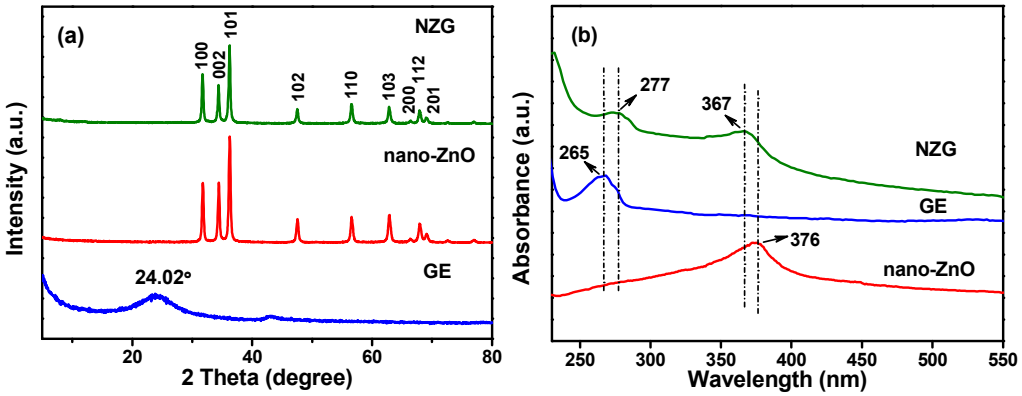

Fig. 2 XRD patterns (a) and UV-vis curves (b) of NZG, GE and nano-ZnO nanocomposites.

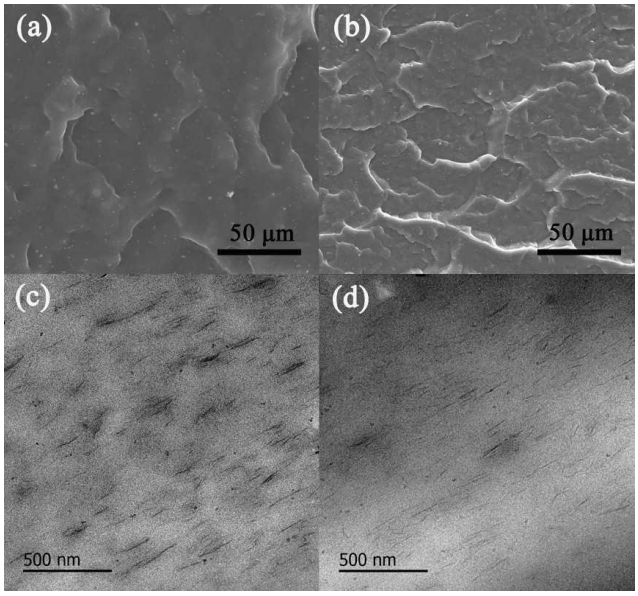

Fig. 3 FESEM images of neat NR (a) and NR/NZG-2.5 nanocomposite (b) after tensile test, and HRTEM images of NR/GE-0.625 (c) and NR/NZG-2.5 (d) nanocomposites.

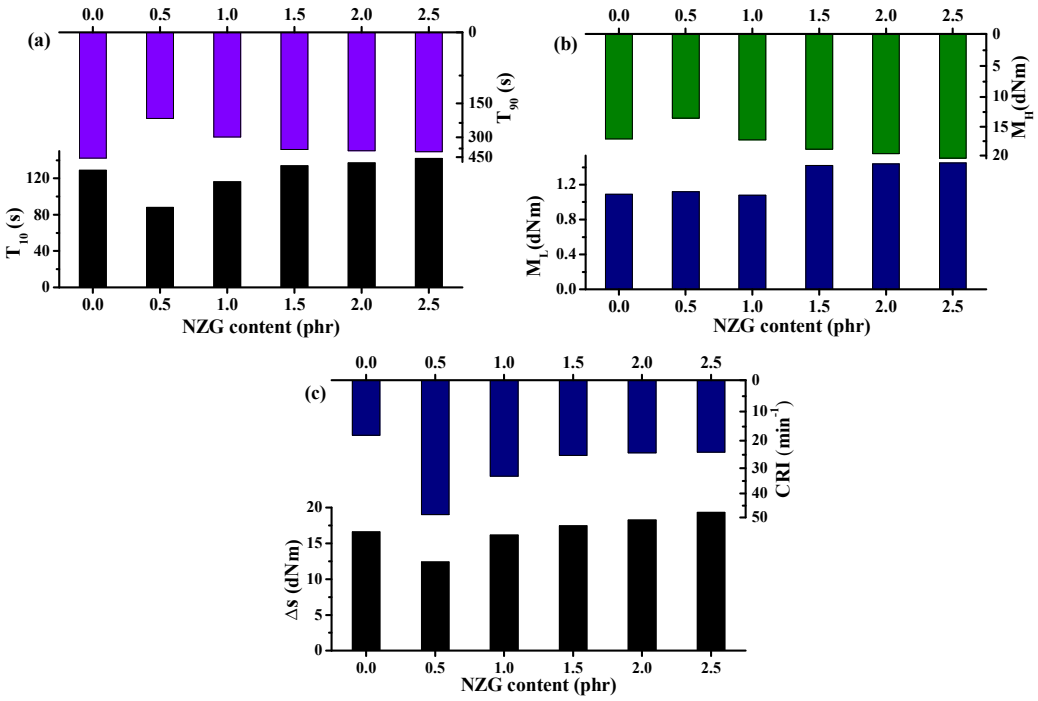

Fig. 4. Vulcanization characteristics of NR/NZG nanocomposites. (a) T_{10} and T_{90}; (b) M_L and M_H; (c) ΔS and CRI.

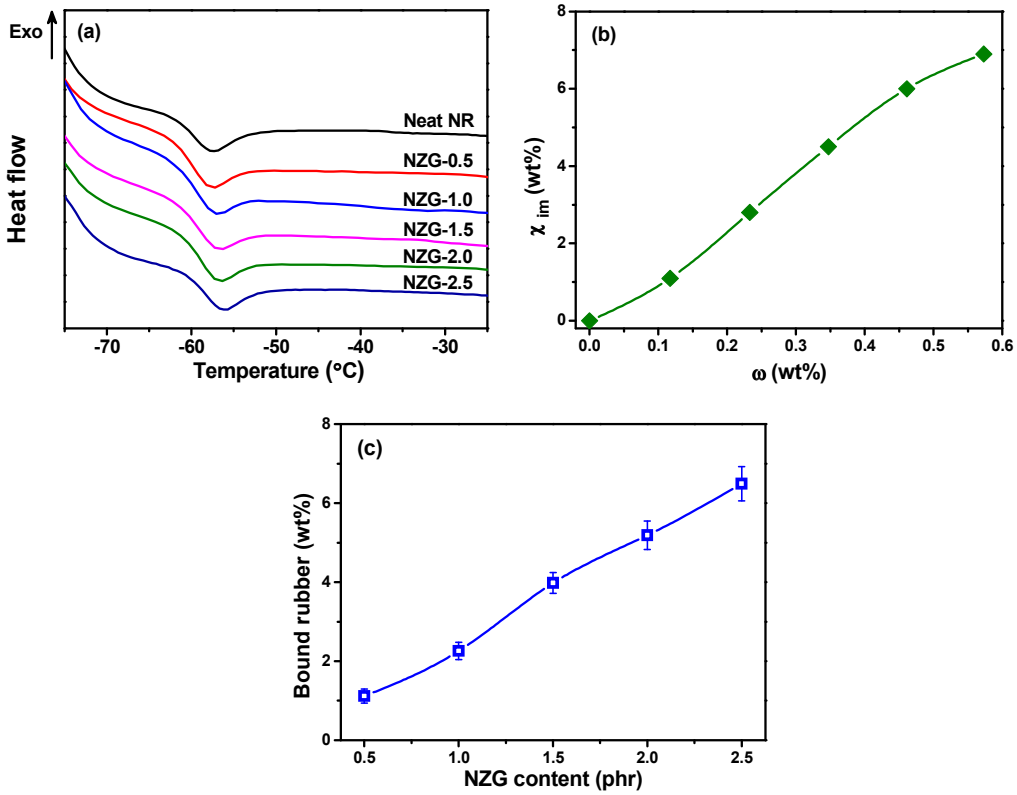

Fig. 5 (a) DSC curves of neat NR and NR/NZG nanocomposites. (b) Weight fraction of immobilized NR (χ_{im}) as a function of weight fraction (ω) of GE. (c) Effect of NZG on the bound rubber content of NR/NZG compounds.

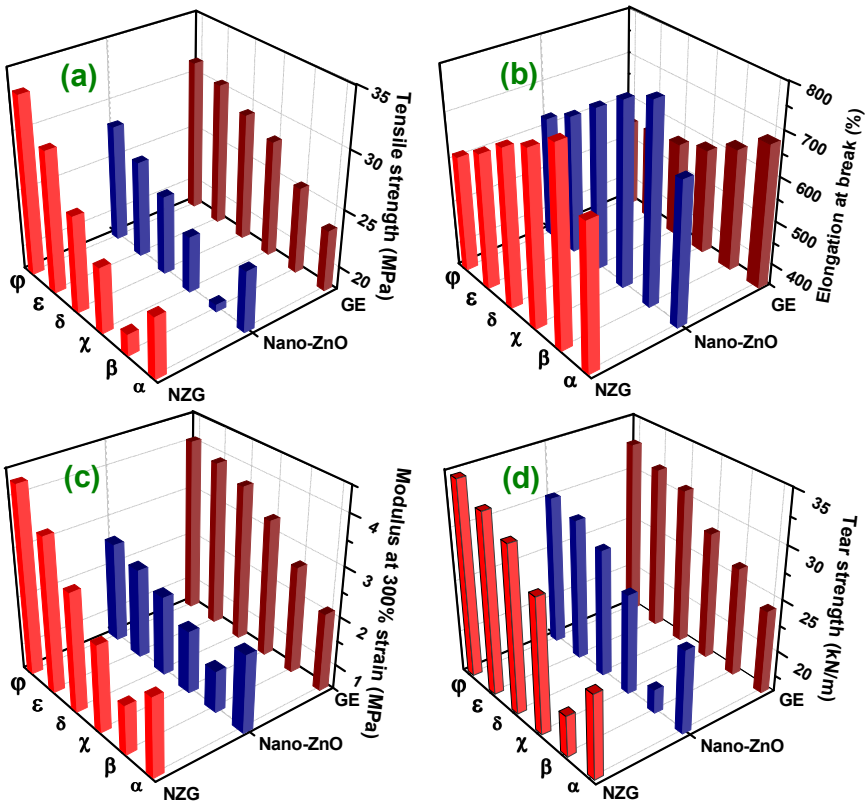

Fig. 6 Comparison of mechanical properties of NR/NZG, NR/Nano-ZnO and NR/GE nanocomposites. (a) Tensile strength; (b) Modulus at 300% strain; (c) Tear strength; (d) Elongation at break. The symbol *α* represents 5 phr for conventional ZnO, and *β, χ, δ, ε, φ* represent 0.5, 1.0, 1.5, 2.0, 2.5 phr for NZG, or 0.375, 0.750, 1.125, 1.500, 1.875 phr for nano-ZnO, or 0.125, 0.250, 0.375, 0.500, 0.625 phr for GE, respecitvely.

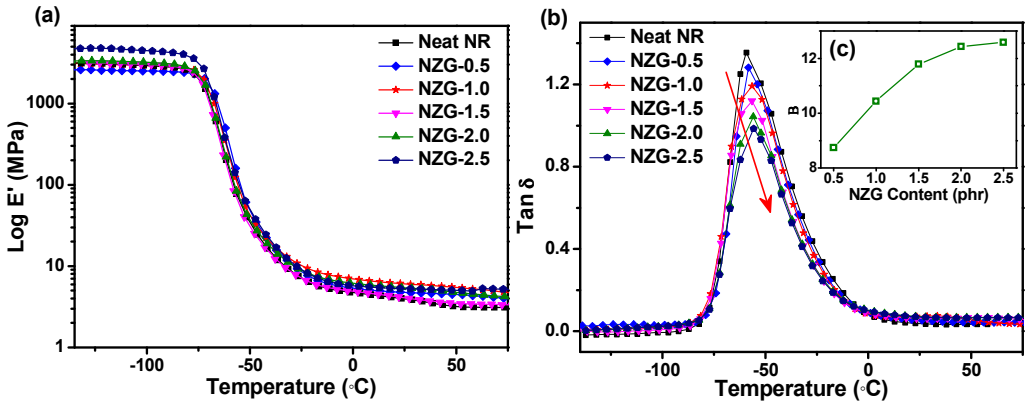

Fig. 7 Storage modulus (a), loss factor (b) and interaction parameter (c) of neat NR and NR nanocomposites with different NZG content.

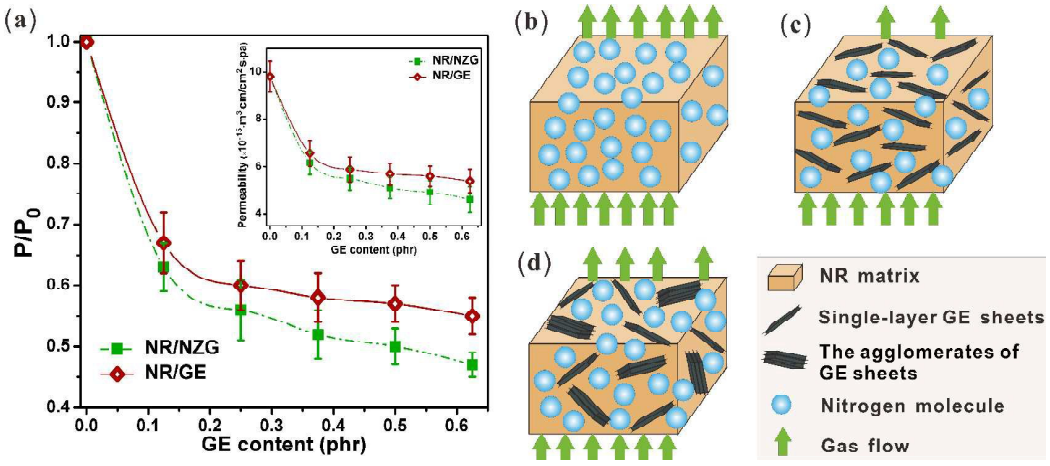

Fig. 8 (a) Nitrogen permeability of NR/NZG and NR/GE nanocomposites normalized by that of neat NR. (b-d) The model of gas flow for neat NR (b), NR/NZG (c) and NR/GE nanocomposites (d). The upper inset shows the absolute values of nitrogen permeability.

Table 1 DSC results for the glass transition of NR/NZG nanocomposites.

Sample	ω^{α} (%)	T_g (K)	ΔT_g (K)	ΔC_p (J/g·K)	ΔC_{pn} (J/g·K)	χ_{im} (wt%)
Neat NR	0	213.65	3.3	0.466	0.466	-
NR/NZG-0.5	0.117	213.65	3.1	0.460	0.461	1.1
NR/NZG-1.0	0.233	213.85	3.2	0.452	0.453	2.8
NR/NZG-1.5	0.347	214.25	3.1	0.443	0.445	4.5
NR/NZG-2.0	0.461	214.45	3.2	0.436	0.438	6.0
NR/NZG-2.5	0.573	214.95	3.4	0.432	0.434	6.9

[α]ω, the weight fraction of GE in the nanocomposites; T_g, the glass transition temperature; ΔT_g, the range of the glass transition; ΔC_p, the heat capacity jump at T_g; ΔC_{pn}, heat capacity jump normalized to the rubber fraction; χ_{im}, the weight fraction of immobilized NR in the nanocomposites.

Table 2 Gas permeability of graphene, graphene oxide, graphite derivative/elastomer nanocomposites.

Elastomer	Filler	Content	Processing	Permeant	Relative reduction (%)
NR[47]	SGO	0.3 (wt%)	Solution	Air	48
SBR[50]	GE	3 (phr)	Latex compounding	Oxygen	67.2
NBR[51]	EG	5 (phr)	Solution	Nitrogen	38
TPU[52]	TRG	1.6 (vol%)	Melt	Nitrogen	52
XNBR[31]	GO	1.9 (vol%)	Latex compounding	Nitrogen	55
NR[42]	rGO	1 (phr)	Latex compounding	Oxygen	36